



# Optics Letters

## Negative refraction in terbium at ultraviolet frequencies

ZACHARY N. BUCKHOLTZ\* AND DENIZ D. YAVUZ

Department of Physics, University of Wisconsin – Madison, 1150 University Avenue, Madison, Wisconsin 53706, USA

\*Corresponding author: buckholtz@wisc.edu

Received 19 June 2020; revised 5 August 2020; accepted 7 August 2020; posted 10 August 2020 (Doc. ID 400358); published 4 September 2020

**One of the key challenges in the development of negative index metamaterials is creating a sufficiently strong magnetic response in the material. Rare-earth ions can contain a strong optical magnetic response even in the ultraviolet region of the spectrum, which can be enhanced using magneto-electric cross-coupling. Using energies, transition strengths, and linewidths from atomic structure software, along with realistic inhomogeneous broadenings and densities in a solid, we simulate a negative index scheme using a terbium crystal at a wavelength of 282 nm.** © 2020 Optical Society of America

<https://doi.org/10.1364/OL.400358>

Over the past couple of decades, the field of metamaterials has made great strides in pushing materials with engineered responses, such as near-zero index materials and negative index materials, to ever shorter wavelengths. From originally operating in the GHz range, metamaterials have advanced into the optical region [1], allowing for exploration into the strange properties and interesting applications that they provide, such as perfect lenses [2], invisibility cloaks [3], and much more [4–6].

Despite their success, metamaterials have several important limitations. Metallic-based metamaterials suffer from high ohmic losses, and face constraints related to the plasma frequency, where the magnetic response saturates and weakens as the plasma frequency is approached [7]. The shortest wavelength at which a negative index can be observed depends on the unit cell size for both metallic- and dielectric-based metamaterials [5]. The size of the unit cell also significantly limits the device performance, e.g., the resolution in perfect lenses. Currently, state-of-the-art structured metamaterials can have unit cells with sizes on the order of 100 nm [1,8,9]. For many exciting applications such as resolving nanoscale objects using a metamaterial lens, a unit-cell size at the nanometer scale is required, which is not possible using current approaches.

Materials based on atomic systems [10–14], specifically rare-earth ions, offer the possibility to overcome these limitations. By using a crystal made of rare-earth ions, the unit cell of the system becomes the unit cell of the crystal, which is on the order of 1 nm, rather than 100 nm. Rare-earth ions are known to have strong magnetic-dipole transitions in the optical and UV

regions of the spectrum [15,16]. In addition, we can take advantage of the quantum mechanical nature of the ions to boost their magnetic response using magneto-electric cross-coupling [17]. Quantum effects can also be used to reduce absorption, providing a transmission window over the frequencies at which the refractive index is negative. Our simulations show that these favorable properties of rare-earth ions, in particular terbium ions, as well as properties of rare-earth-ion-based stoichiometric crystals, are capable of producing an atomic-based metamaterial with a negative index of refraction.

Strong magnetic responses in atomic systems at optical frequencies are rare, and even those in rare-earth ions are not strong enough to produce a negative permeability, which is the most direct route to negative refraction. However, we can enhance the magnetic response by coherently coupling it to the system's electric response, using a process called magneto-electric cross-coupling [17].

The electric response used for the cross-coupling needs to occur at the same frequency as the magnetic response. While strong magnetic responses at optical frequencies are hard to come by, it is even more rare to find one at the same frequency as an electric response. Our scheme overcomes this limitation by using two Raman transitions, one absorbing and one amplifying, to construct an electric response with minimal absorption at the required frequency [18]. These two Raman transitions can be very far detuned from the electric-dipole transition, thereby circumventing the requirement that both electric and magnetic-dipole transitions should be at the same frequency.

Rare-earth-ion based materials can provide the properties needed to implement our negative index scheme. Most importantly, rare-earth ions are known to have strong, narrow magnetic-dipole transitions, with calculations going back to the 1960s [15,16] and recent experimental confirmation of a strong magnetic-dipole transition in trivalent europium at a wavelength of 527.5 nm [19,20]. Using Robert Cowan's atomic structure code [21], we have identified the  ${}^7F_6 \rightarrow {}^5F_5$  transition in  $Tb^{+3}$  as a strong magnetic-dipole transition at a wavelength of 282 nm. In addition, Cowan's code shows that the terbium ion's excited  $4f^7 5d^1$  configuration, shown in the top of Fig. 1, has states at significantly lower energies than the other rare-earth ions with similarly strong magnetic transitions, allowing for stronger Raman transitions to construct our electric response. These two properties together make terbium an

excellent candidate for implementing a negative index in a real atomic system.

An energy level diagram for our scheme can be found in the bottom of Fig. 1, which is similar to what was first discussed in Ref. [22]. The transition between states  $|g\rangle$  and  $|m\rangle$  is the magnetic-dipole transition that provides the magnetic response. The Raman transitions involve states from the first excited configuration,  $|e\rangle$ , and the two lower states  $|1\rangle$  and  $|2\rangle$ . States  $|g\rangle$ ,  $|1\rangle$ , and  $|2\rangle$  are hyperfine states of the  ${}^7F_6$  state, and state  $|m\rangle$  is the  ${}^5F_5$  state. By altering the intensity and frequency of the control beams,  $E_{c1}$  and  $E_{c2}$ , we can control the strength and frequency of the electric response. The cross-coupling is implemented by the beam  $\Omega_{2m}$ , which couples together the magnetic and electric responses.

By coupling together the electric and magnetic responses, the polarization and magnetization of the material are altered:

$$P = \epsilon_0 \chi_E E + \frac{\xi_{EB}}{c\mu_0} B, \quad (1)$$

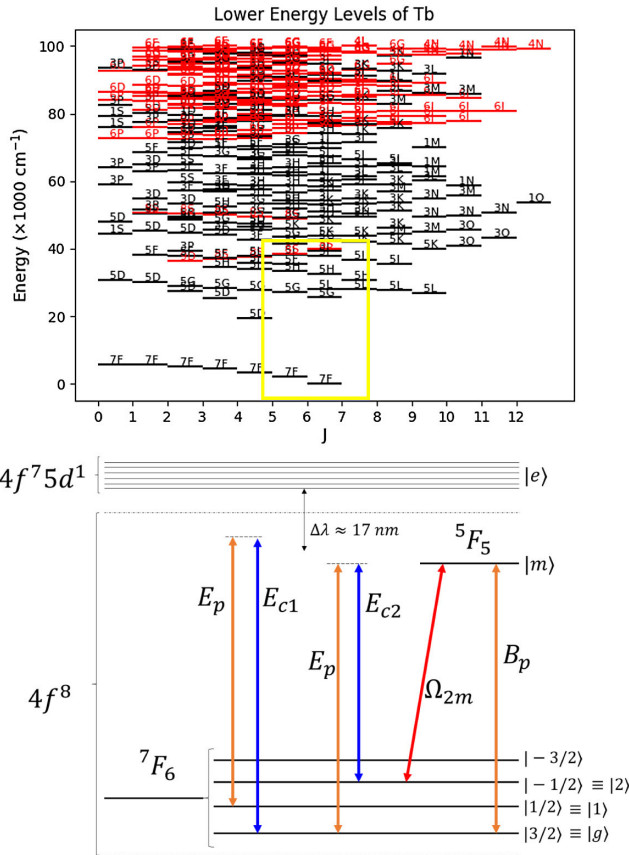


**Fig. 1.** (top) Energy levels for the free terbium ion calculated with Cowan's code. The  $4f^8$  configuration states are black, and the  $4f^75d^1$  configuration states are shown in red. Several of the  $4f^75d^1$  states occur at much lower energies than other trivalent rare-earth ions with comparable magnetic-dipole transitions. The yellow box encloses most of the levels in our negative index scheme. (bottom) Energy level diagram of our magneto-electric cross-coupling scheme in terbium [18]. The magnetic response, derived from a two-level transition between states  $|g\rangle$  and  $|m\rangle$ , is enhanced by the cross-coupling beam  $\Omega_{2m}$ , which couples the magnetic response to the two Raman transitions controlled by beams  $E_{c1}$  and  $E_{c2}$ .

$$M = \frac{\xi_{BE}}{c\mu_0} E + \frac{\chi_M}{\mu_0} B, \quad (2)$$

where the  $\xi$  are the magneto-electric cross-coupling coefficients. A system with this sort of cross-coupling will have an index of refraction

$$n = \sqrt{\epsilon\mu - \frac{(\xi_{EB} + \xi_{BE})^2}{4}} + \frac{i}{2}(\xi_{EB} - \xi_{BE}). \quad (3)$$

By coherently adjusting the  $\chi$ 's and the  $\xi$ 's, we can obtain a negative index of refraction with a much weaker magnetic response than we would need with no cross-coupling [17,23].

The forms, along with their derivations, of the susceptibilities and cross-coupling coefficients for our scheme can be found in Ref. [24]. In order to successfully implement this model in a real system, the system needs to have four important properties: a strong magnetic transition, narrow linewidths, high densities, and strong Raman transitions.

Rare-earth ions have traditionally been utilized mostly as dopants in a crystal host matrix. An important property of rare-earth ions is that the strong, narrow homogeneous linewidths of the free ions tend to remain strong and narrow even when doped into as solid. In addition, rare-earth ion dopants experience relatively small inhomogeneous broadenings due to shielding from the  $5s$  and  $5p$  shells [16,25]. Unfortunately, the narrowest inhomogeneous broadenings, required for our negative index scheme, come at the price of reduced density [26,27]. As it turns out, the densities with low enough inhomogeneous broadening are too low for our negative index scheme, making it seem as though doped crystals are not a suitable candidate to implement our negative index scheme. However, stoichiometric crystals could offer the best of both worlds; rare-earth-ion-based stoichiometric crystals have been observed to have narrow inhomogeneous broadenings (25 MHz) with densities around  $4 \times 10^{27} \text{ m}^{-3}$  [28,29]. With these properties, it is possible to produce a negative index.

We ran simulations of this negative index scheme with the ionic parameters from Cowan's code and the bulk parameters from a typical stoichiometric crystal [29]. The magnetic-dipole moment of the  ${}^7F_6 \rightarrow {}^5F_5$  transition was set to the value calculated by Cowan's code,  $\mu = 0.09\mu_B$ . The magnetic-dipole transition's homogeneous linewidth was set to  $2\pi \times 2000$  Hz, a typical value for the phonon-induced relaxation rate at cryogenic temperatures. This linewidth was augmented by a 25 MHz inhomogeneous linewidth. The Raman coupling coefficient was determined by summing over the entire  $4f^75d^1$  configuration:

$$C = \frac{1}{2\hbar^2} \sum_e \frac{d_{ge}d_{ef}^*}{\omega_{ge} - \omega_p - i\Gamma_e}, \quad (4)$$

where the excited configuration state electric-dipole moments,  $d_{ge}$  and  $d_{ef}$ , transition frequency from the ground state,  $\omega_{ge}$ , and linewidth,  $\Gamma_e$ , are all taken from Cowan's code.  $\omega_p$  is the frequency of the magnetic transition. The result of carrying out this sum is  $C = 3.6 \times 10^{-6} + 6.0 \times 10^{-12}i \text{ Hz m}^2/\text{V}^2$ . The hyperfine states were taken to have an inhomogeneous broadening of 50 kHz, which is typical of rare-earth ion hyperfine states in solids [30–32]. The control laser beam intensities and the cross-coupling rate need to be tuned accurately to produce the desired interference. For the results presented below, we set these

values to be  $I_{c1} = 11.175 \text{ MW/cm}^2$ ,  $I_{c2} = 18 \text{ MW/cm}^2$ , and  $\Omega_{2m} = 2\pi \times 2.5 \text{ MHz}$ . Further details on our simulations can be found in Ref. [33].

In our simulations, we first investigated the density dependence, as well as the ability to produce a negative index with low absorption. Representative results for the refractive index as the probe laser frequency is varied at different densities are shown in Fig. 2. We observe that there is indeed a narrow transparency window when the index of refraction goes below zero and the

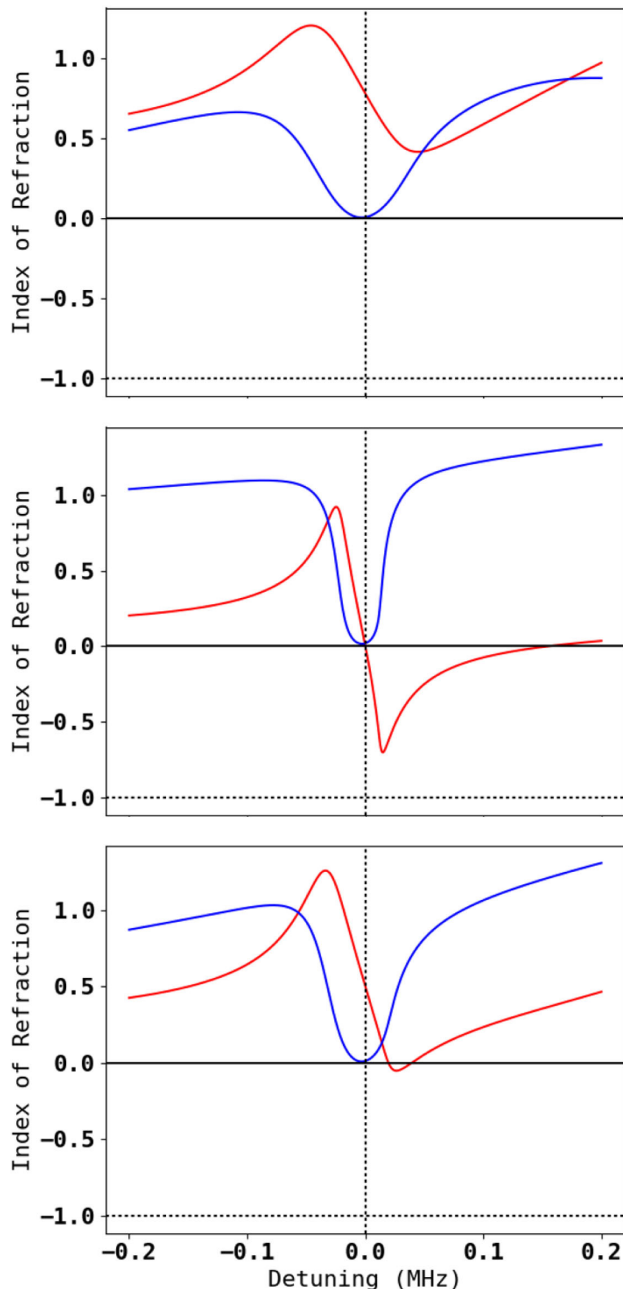


**Fig. 2.** Index of refraction frequency sweep in  $\text{Tb}^{+3}$  in a stoichiometric crystal for three different densities. Starting at the top left and going clockwise, the densities are  $4 \times 10^{26} \text{ m}^{-3}$ ,  $1 \times 10^{27} \text{ m}^{-3}$ , and  $2.5 \times 10^{27} \text{ m}^{-3}$ . The real part of the index of refraction is in red, and the negative of the imaginary part is blue. The parameters used to make this plot were taken from Cowan's code and from typical values for stoichiometric crystals. See text for details.

absorption is relatively small. As the density increases, we see in Fig. 2 that the transparency window becomes sharper, and the index of refraction shifts to more negative values. Figure 3 shows the variation of the index of refraction as the ionic density is changed. The top plot shows the real and imaginary parts of the index when the absorption is minimized. The bottom plot shows the real and imaginary parts when the real part is minimized. We find that the index of refraction first goes negative at around  $1 \times 10^{27} \text{ m}^{-3}$ , and the index at the frequency of least absorption first goes negative around  $3 \times 10^{27} \text{ m}^{-3}$ .

Since the results of our simulation depend on the inhomogeneous linewidth and the density, we considered whether a more negative index could be achieved by implementing ion-class selection [34] to reduce the inhomogeneous linewidth at the cost of lower density. The results of our index versus inhomogeneous broadening simulations are shown in Fig. 4. In this figure, the reduction in ionic density was proportional to the reduction in inhomogeneous linewidth. For example, the simulation run with an inhomogeneous broadening of 5 MHz was run with an ionic density of one-fifth the full value. The results shown in Fig. 4 show the index of refraction when absorption is minimized (top) and when the index of refraction is at a minimum (bottom).

Figure 4 shows that although our scheme relies on both narrow linewidths and high density, it is more important to have high density at the cost of wider inhomogeneous broadenings. In addition, we see that near-zero indices can produce figures of merit,  $F = -\text{Re}[n]/|\text{Im}[n]|$ , as high as 10. We also see that

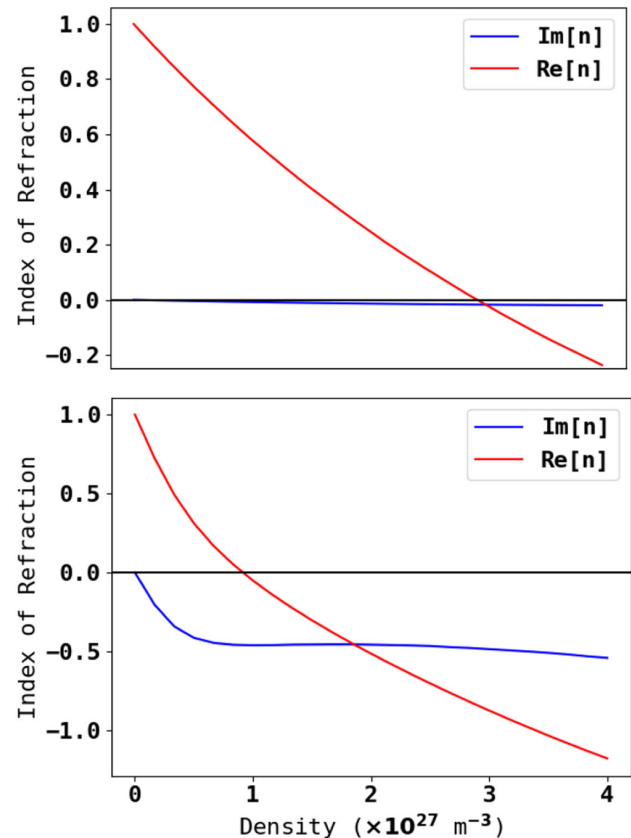


**Fig. 3.** Real and imaginary parts of the index of refraction as the ionic density is varied. The top plot shows the real and imaginary parts at the frequency with minimum absorption. The bottom plot shows the real and imaginary parts when the real part is at a minimum.

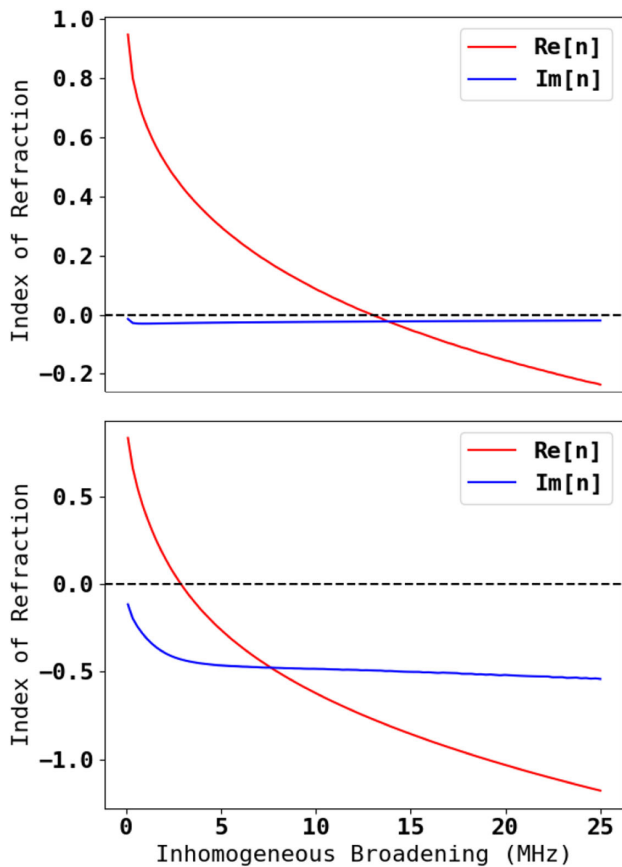


**Fig. 4.** Index of refraction versus inhomogeneous broadening with the density adjusted to account for the narrower linewidth. On top is a plot of  $\text{Re}[n]$  and  $\text{Im}[n]$  at the point where the real part is most negative. In the bottom plot, we have  $\text{Re}[n]$  and  $\text{Im}[n]$  for when absorption is at a minimum.

if we allow for higher absorption, resulting in a figure of merit around two, much lower indices, down to and below  $n = -1$ , are possible.

We note that while we have discussed the refractive index of a terbium crystal, we have not investigated the length over which such an index can be obtained. The practical limit on the crystal length will likely be determined by the absorption/gain on the probe laser beam, which will depend on the imaginary part of the refractive index,  $\text{Im}[n]$ . As shown in Figs. 3 and 4, for a reasonable range of parameters we have  $\text{Im}[n] \sim 0.1$ . The probe wave can propagate over a length of  $L \sim \lambda/\text{Im}[n]$  before it is largely absorbed. This would then put the length over which we would expect our results to apply to  $L \sim 10\lambda$ , which is about  $3 \mu\text{m}$ . The extension of our results to optically thick crystals is currently an open question. A further discussion of various practical aspects of rare-earth systems can be found in Ref. [22].

In conclusion, we simulated a negative index scheme based on magneto-electric cross-coupling in an atomic based metamaterial. The magnetic response was supplied by trivalent terbium ions, which have favorable properties for our scheme including a strong magnetic transition in the UV and low-lying energy levels from the  $4f^7 5d^1$  configuration. The terbium ions were incorporated into a stoichiometric crystal, and typical densities and inhomogeneous broadenings were included in our simulations. The results of our simulation showed that a near-zero index

material could be achieved with low absorption, or an index of  $n = -1$  could be achieved with increased absorption. Given that the negative index in our scheme occurs at a wavelength of 282 nm, successful implementation in the laboratory would push negative indices far beyond the current state-of-the-art metamaterials.

**Funding.** University of Wisconsin–Madison

**Disclosures.** The authors declare no conflicts of interest.

## REFERENCES

1. Y. Liang, Y. Zhiyong, R. Ningjuan, Q. Sun, and T. Xu, *Opt. Lett.* **42**, 3239 (2017).
2. J. B. Pendry, *Phys. Rev. Lett.* **85**, 3966 (2000).
3. U. Leonhardt, *Science* **312**, 1777 (2006).
4. V. G. Veselago, *Sov. Phys. Usp.* **10**, 509 (1968).
5. S. A. Ramakrishna, *Rep. Prog. Phys.* **68**, 449 (2005).
6. I. Liberal and N. Engheta, *Nat. Photonics* **11**, 149 (2017).
7. R. S. Penciu, M. Kafesaki, T. Koschny, E. N. Economou, and C. M. Soukoulis, *Phys. Rev. B* **81**, 235111 (2010).
8. L. Y. M. Tobing, L. Tjahjana, D. H. Zhang, and Q. Zhang, *Adv. Opt. Mater.* **2**, 280 (2014).
9. S. Jahani and Z. Jacob, *Nat. Nanotechnol.* **11**, 23 (2016).
10. M. O. Oktel and O. E. Mustecaplioglu, *Phys. Rev. A* **70**, 053806 (2004).
11. Q. Thommen and P. Mandel, *Phys. Rev. A* **96**, 053601 (2006).
12. P. P. Orth, R. Hennig, C. H. Keitel, and J. Evers, *New J. Phys.* **15**, 013027 (2013).
13. A. P. Fang, W. Ge, M. Wang, F. Li, and M. S. Zubairy, *Phys. Rev. A* **93**, 023822 (2016).
14. M. T. Trinh, K. Makhal, E. F. C. Dreyer, A. Shanker, S. J. Yoon, J. Kim, and S. C. Rand, *Opt. Express* **27**, 21295 (2019).
15. B. G. Wybourne and L. Smentek, *Optical Spectroscopy of Lanthanides: Magnetic and Hyperfine Interactions* (Taylor & Francis, 2007).
16. G. H. Dieke and H. M. Crosswhite, *Appl. Opt.* **2**, 675 (1963).
17. J. Kastel, M. Fleischhauer, S. F. Yelin, and R. L. Walsworth, *Phys. Rev. A* **79**, 063818 (2009).
18. D. E. Sikes and D. D. Yavuz, *Phys. Rev. A* **82**, 011806 (2010).
19. M. Kasperczyk, S. Person, D. Ananias, L. D. Carlos, and L. Novotny, *Phys. Rev. Lett.* **114**, 163903 (2015).
20. N. R. Brewer, Z. N. Buckholtz, Z. J. Simmons, E. A. Mueller, and D. D. Yavuz, *Phys. Rev. X* **7**, 011005 (2017).
21. R. Cowan, *The Theory of Atomic Structure and Spectra* (University of California, 1981).
22. D. D. Yavuz and Z. N. Buckholtz, *Advances in Atomic, Molecular, and Optical Physics* (Academic Press, 2018), Chap. 8.
23. J. Kastel, M. Fleischhauer, S. F. Yelin, and R. L. Walsworth, *Phys. Rev. Lett.* **99**, 073602 (2007).
24. D. E. Sikes, "Theoretical schemes for negative refraction and enhanced refractive index in atomic systems," Ph.D. thesis (University of Wisconsin–Madison, 2012).
25. R. M. Macfarlane, *J. Lumin.* **100**, 1 (2002).
26. R. Macfarlane and R. Meltzer, *Phys. Rev. B* **58**, 5692 (1998).
27. C. W. Thiel, T. Bottger, and R. L. Cone, *J. Lumin.* **131**, 353 (2011).
28. R. L. Ahlefeldt, M. R. Hush, and M. J. Sellars, *Phys. Rev. Lett.* **117**, 250504 (2016).
29. R. L. Ahlefeldt, M. J. Pearce, M. R. Hush, and M. J. Sellars, *Phys. Rev. A* **101**, 012309 (2020).
30. A. Arcangeli, M. Lovrić, B. Tumino, A. Ferrier, and P. Goldner, *Phys. Rev. B* **89**, 184305 (2014).
31. K. Holliday, M. Croci, E. Vauthey, and U. P. Wild, *Phys. Rev. B* **47**, 14741 (1993).
32. M. Lovrić, P. Glasenapp, and D. Suter, *Phys. Rev. B* **85**, 014429 (2012).
33. Z. N. Buckholtz, "Progress towards an atomic metamaterial," Ph.D. thesis (University of Wisconsin–Madison, 2020).
34. M. Nilsson, L. Rippe, S. Kröll, R. Klieber, and D. Suter, *Phys. Rev. B* **70**, 214116 (2004).